Available online at www.sciencedirect.com

ScienceDirect

Procedia CIRP 111 (2022) 536–540

www.elsevier.com/locate/procedia

12th CIRP Conference on Photonic Technologies [LANE 2022], 4-8 September 2022, Fürth, Germany

Laser welding for stamping blank reinforcement: Signal monitoring for digital certification

Oihane Murua[a,*], Jon Iñaki Arrizubieta[a], Aitzol Lamikiz[a], Lander Galdos[b]

[a]*University of the Basque Country UPV/EHU, Plaza Ingeniero Torres Quevedo 1, 48013 Bilbao, Spain*
[b]*Mondragon University, Loramendi 4; 20500 Arrasate – Mondragón, Spain*

* Corresponding author. Tel.: +34-94-601-7347. *E-mail address:* oihane.murua@ehu.eus

Abstract

Sheet metal stamping is widely used in the automotive sector, where the thickness of the blanks is critical to reduce the final weight of the manufactured part. Nevertheless, in specific locations, reinforcements are required for achieving the desired properties. In view of this necessity, laser welding is proposed to reinforce blanks prior to the stamping operation, which enables to increase the mechanical resistance of the stamped part in the required areas without penalizing the total weight. HCT780C (also called DP780) is the material employed in the present study and T-joints are analyzed. The welding process is monitored by means of a coaxial camera and a two-colour pyrometer. In parallel, the cross-sections of the welds are analyzed to evaluate any internal defect or lack of fusion and shear tests are performed to ensure the correct functioning of the weld. The combination of both results provides the opportunity for developing a digital certification of the welding process, which will enable the verification of future welds without the need for experimental studies.

Keywords: laser welding, blank, reinforcement, monitoring;

1. Introduction

In the automotive industry, weight reduction is a differential factor [1] and for this purpose laser welding (LW) is being widely used in different applications. Thanks to the high penetration, low distortion, and high flexibility that the LW offers, high-quality weld joints can be attained [2]. However, the result of the LW depends on a series of complex physical phenomena, such as laser-metal interaction, melting and solidification, keyhole formation, and molten material movements. Therefore, monitoring systems are required for ensuring the quality of the weld.

Ex-situ monitoring techniques are useful for detecting defects during the part post-processing, but in-situ monitoring techniques enable the determination of the quality of weld during the joining process [3]. Nevertheless, as Allen et al. stated, there is a lack of in-situ monitoring tools [4]. The in-situ monitoring of LW presents a series of challenges principally related to the fast nature of the process and the noise produced by the plasma plume and the projections.

Most employed monitoring systems are based on optical imaging because they enable contactless measuring. Photodiode, camera, pyrometer, and tomography techniques have already been used. For instance, two-colour pyrometers have been used for measuring the temperatures of the melt pool [5], and coaxial monitoring systems in the VIS and NIR spectrum for obtaining real-time images of the welding process [6]. More complex techniques, such as inline coherent imaging (ICI), have also been employed for in-situ monitoring the depth of the keyhole [3].

Commonly employed materials in automotive applications are the Dual-Phase (DP) steels, which consist of ferrite and martensite, soft and hard phases respectively, and thanks to their mechanical properties, they enable lightweight structures [7]. An example of a widely used DP steel is the DP780. The microstructure and mechanical properties of LW DP780 steels

10.1016/j.procir.2022.08.086

have been already discussed in previous works. Di et al. concluded that in tensile tests the softening zone adjacent to the welding zone did not influence the tensile properties of the weld joints [7]. However, Gao et al. concluded that the lower the heat input the better properties of the DP780 base material are ensured [1]. Therefore, by certifying proper welding conditions, good performance of the weld is also guaranteed, and effort in monitoring and digital certification of the process should be done.

In the present work, a dual LW in-situ monitoring system is implemented based on a two-colour pyrometer and a coaxial camera for a T-joint welding process. Measured signals have been related to the quality and shape of the obtained welds and a digital inspection system is developed. The digital inspection aims to provide a digital certification based on the in-situ monitoring of whether a weld is sound without the need for ex-situ experimental analysis.

2. Methodology

2.1. Materials and equipment

The HCT780C (also called DP780) steel employed in the tests is supplied by Gonvarri Industries. The thickness of cold-rolled DP780 is 1.5 mm and two sheets have been fabricated: (a) 90x20 mm^2 and (b) 150x50 mm^2 (being the longest side the rolling direction) The chemical composition of DP780 is listed in Table 1.

Table 1. Chemical composition of the as-received DP780 steel (wt.%).

C	Mn	Si	P	Al	Nb
0.13	1.48	0.19	0.007	0.05	0.015
V	S	Ti	Cu	Cr	Fe
0.009	0.0034	0.002	0.0194	0.07	Bal.

For the laser welding tests a Nd:YAG solid-state laser with a maximum power of 1 kW in CW from Coherent-Rofin is used. A 200 mm focusing optic is used and at the working plane, the laser beam has a 0.6 mm diameter spot. The welding head is mounted on a five-axis laser centre and an Argon 2X protective gas supplied by Nippon Gases is used in the upper and lower faces of the sheets. The laser power has been calibrated with a power meter prior to the welding tests, and power losses are reported below 2%, which permits to assume that the programmed laser power is the nominal.

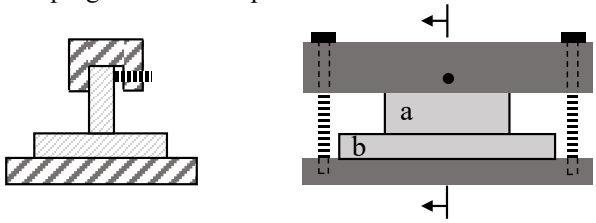

Fig. 1. Experimental setup for the DP780 sheet welding, with bolted joints.

2.2. Experimental tests

A T-joint welding strategy is selected for the digital monitoring validation, being the final aim the use of T-welded stringer precuts to stamp lighter components [8,9]. The biggest DP780 sheet (b) is placed in the flat position and the smallest (a) as a vertical stiffener. The tool shown in Fig. 1 is employed to press the top sheet (a) towards the button sheet (b) and the the welding strategy consists of two weld beads on both sides of the T-joint.

2.3. Mechanical tests

The shear bonding strength is measured using a shear tool developed for this project, which is mounted in a universal testing machine from Instron with a maximum load of 100 kN. The setup is schematically illustrated in Fig. 2. The specimen in clamped horizontally in the tool after being EDM cut to a length of 20 mm and the shear punch is moved with a constant velocity of 1 mm/s. During the test, force and displacement are recorded.The shear bonding strength σ_s can be calculated using equation (1), where the maximum shear force F_{max} is divided by the initial shear area A_s of the reinforcement [8].

$$\sigma_s = F_{max} / A_s \quad (1)$$

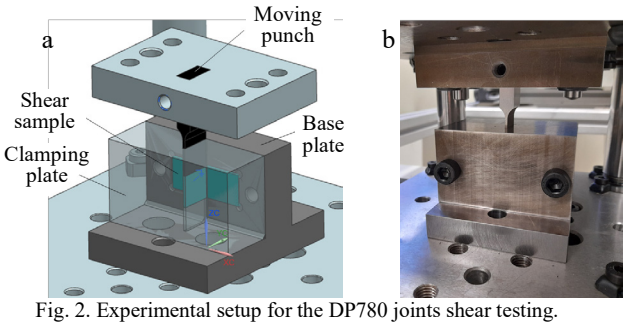

Fig. 2. Experimental setup for the DP780 joints shear testing.

3. Monitoring system

The employed dual monitoring system consists of a coaxial camera and a two-colour pyrometer, which simultaneously extract data from the process.

The selected VIS/NIR Imaging camera to capture the melt pool geometry is a CS135MUN from Thorlabs. This sensor has a 1.3MP resolution and a NIR enhanced CMOS sensor with a 220 fps maximum acquisition frame rate. The camera is connected to a dichroic mirror that provides an alternate coaxial optical path to the laser in order to allow visualizing the focal plane. The camera is connected to a PC through USB3.0 and the obtained images are processed in Matlab R2021. This setup provides a fast image processing system and allows to evaluate the LW process in-situ. The non-contact temperature measurement is performed by means of the IGAR 12-LO two-colour pyrometer. The measuring range is between 500-2500 ºC and results are sent directly to the PC.

4. Obtained results

4.1. Experimental results

After a visual inspection of the weld beads, the three regions described in Fig. 3 are differentiated. For low laser powers and high machine feed rates, the energy density of the laser is not enough for joining both sheets, whereas, for high laser powers and low feed rates, the laser pierces the DP780 sheets. Consequently, there is a central band, where a proper weld can be obtained.

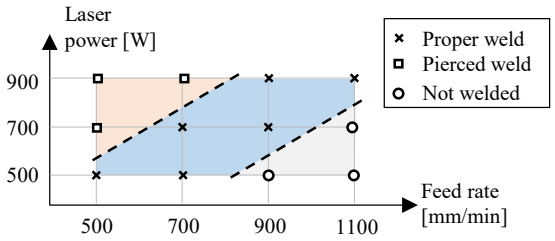

Fig. 3. Summary of the experimental tests.

Depending on the process parameters the welding mechanism varies from conduction to keyhole. To represent the different mechanisms of the welding process, in Fig. 4 three weld beads are shown. The image on the left side (a) represents the weld with the lowest power and feed rate, whereas the one on the right (c) represents the highest process parameters.

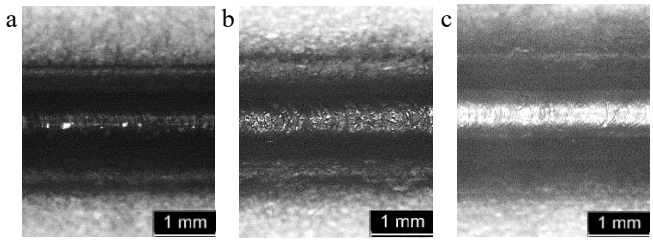

Fig. 4. Upper views of the weld beads: (a) 500 W and 500 mm/min; (b) 700 W and 900 mm/min; (c) 900 W and 1100 mm/min.

After the visual inspection, the samples are cross-sectioned in the centre, polished, and attacked chemically with Nital 4 to reveal the microstructure of the DP780. In Fig. 5 three metallographs are presented: conduction mode welding (a), keyhole welding (c), and mixed-mode welding (b).

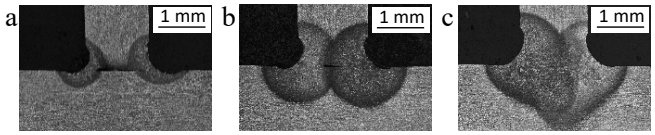

Fig. 5. Cross section of the weld beads: (a) 500 W and 500 mm/min; (b) 700 W and 900 mm/min; (c) 900 W and 1100 mm/min.

No pores are detected inside the weld region, this is, the material is molten by the laser. Nevertheless, if the bead penetration is not enough, Fig. 5(a) and (b), there is a gap between the two DP780 sheets that will affect negatively the mechanical resistance of the joint.

4.2. Data analysis

The first step of the data analysis is to process the images obtained by means of the coaxial camera. The obtained images are filtered and averaged by the previous frames. For the filtering process, a Matlab code is developed. The image processing starts by reading a welding video, which was recorded in 'AVI' format, in order to obtain all the meaningful frames. That is to say, all black frames are deleted because they just represent the pre- and post-welding moments, when the laser is off, and are not relevant for the melt pool inspection. Afterward, each video frame or image is converted into a grayscale image, where each pixel has a value between 0 and 255. To extract the melt pool geometry a binarization algorithm is used with a high threshold value, which is set at 250. Once the binarization is done, the image is averaged with the previous frames. Finally, a second threshold filter is implemented for obtaining a more accurate weld pool geometry with the averaged image. The Matlab code takes around 1 minute for a 90 mm weld length in a conventional Intel i5 PC.

As it can be seen in Fig. 6, the number of employed frames in the averaging has a relevant effect on the stability of the monitored signal. The 10 frames averaging algorithm results in a stable weld-width signal. Therefore, this value is employed in all tests.

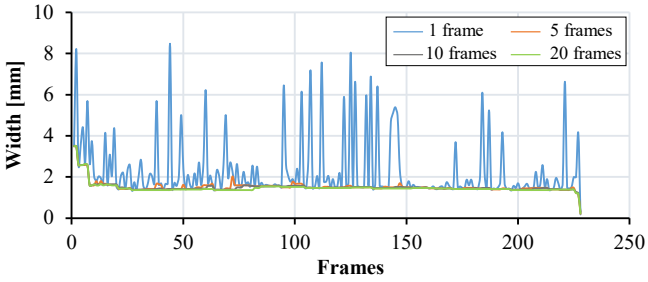

Fig. 6. Image processing results for the 900W laser power and 1100 mm/min feed rate test at different averaging number of frames.

In order to illustrate the performance of the filtering algorithm, in Fig. 7 (a) the image extracted from a certain frame of the video, (b) the averaged image, and (c) the filtered image are shown.

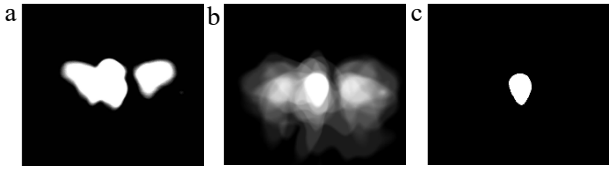

Fig. 7. Image processing result for 900 W and 1100 mm/min weld at the 3.0 s time instant from the weld beginning: (a) Image without treatment; (b) Averaged image of 10 frames; (c) Filtered image.

The data obtained by the non-contact pyrometer is shown in Fig. 8, where the commented two welding modes can be distinguished. The 700W-900mm/min temperature profile shows a mixed welding mechanism, as it can be seen LW starts in a conduction mode but when temperatures between 1900-2000 ºC are reached, LW changes to keyhole mode and a sudden rise of the temperature occurs. A similar phenomenon is detected in the 500W-500mm/min weld. On the contrary, for the 900W laser power temperatures above 2000 ºC are obtained during the whole process and a constant keyhole mechanism is measured.

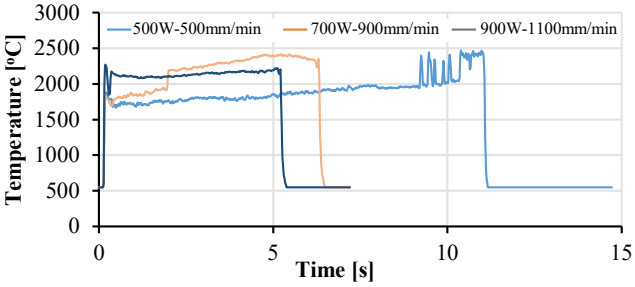

Fig. 8. Temperatures measured by the two-colour pyrometer.

Therefore, if a constant keyhole LW mechanism is desired, temperatures above 2000 ºC must be ensured for the DP780. On the contrary, for guaranteeing a conduction welding

mechanism temperatures must be maintained below 1900 ºC through a close-loop laser-power control.

4.3. Monitoring validation

For the validation of the dual monitoring system, on the one hand, the width of the weld beads is compared with the width provided by the coaxial camera. On the other hand, the signal variation when changing from conduction to keyhole welding is studied. Fig. 9 shows the correlation between the monitored signals and the experimental width.

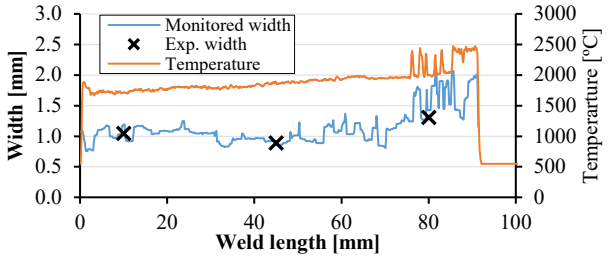

Fig. 9. Comparison between the monitored and experimental width and the correlation with the temperature signals for the 500 W - 500 mm/min test.

As a second and contrary result, in Fig. 10 the monitored bead width and the experimentally measured values are shown, as well as the shape of the monitored melt pool after the image treatment.

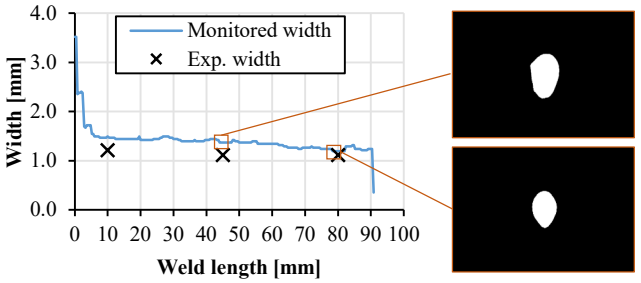

Fig. 10. Comparison between the monitored and experimental width for a 900 W laser power and an 1100 mm/min feed rate.

In keyhole welding, the LW process is unstable and so happens with the monitored signal. Therefore, in the first instants, the weld width is overpredicted until the filtering algorithm stabilizes the process.

4.4. Mechanical evaluation

Besides the microstructural properties, the mechanical properties of the laser-welded joints like the bonding strength are of special interest for a proper stamping of these kinds of stringer precuts.

The bonding joint strength is investigated by shear tests. Based on the maximum shear force and the initial area of the welded stringer the shear strength is calculated according to equation (1).

An exemplary curve of the shear test and the tested sample are shown in Fig. 11. As it is observed, a maximum shear force is reached at a given punch displacement, which indicates the start of the weld failure. After this peak, a separation of the welded plate occurs and friction force with the tool and deformed (thickened) sample occurs. The average maximum shear stress for five different tests is 599.7 MPa with a standard deviation of 9.5 MPa. Maximum force peak occurs at a punch displacement of 3.15 mm with a standard deviation of 0.08 mm.

The shear stress measured during the experimental tests is higher than the theoretical von Mises shear stress of the base material. With an Ultimate Tensile Strength (UTS) of 833 MPa, the theoretical shear stress of the material is 481 MPa ($\frac{UTS}{\sqrt{3}}$). The displacement at failure also indicates a sufficiently ductile behavior of the weld joint and so these process parameters are considered suitable for the production of T-welded stringer sheets for their subsequent stamping of lightweight components.

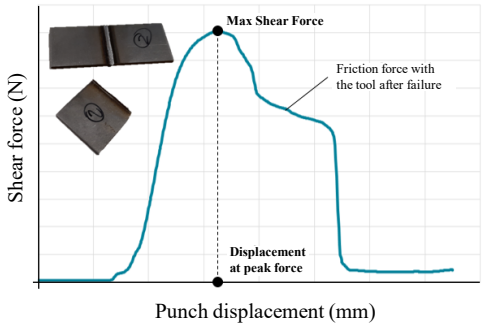

Fig. 11. Exemplary experimental force-displacement curve of the shear test and tested sample.

5. Conclusions

In the present work a dual monitoring system capable of certifying digitally whether the LW is sound has been developed and validated. The system analyses the data obtained in-situ, but since the data processing time is longer than that of the actual LW process, it cannot be used for controlling the process parameters in closed-loop. Nevertheless, it has been proven useful for ensuring the quality of the welds. The measured temperatures and their stability provide the information required for defining the welding mechanism (keyhole or conduction), whereas the coaxial camera images are used for determining the width of the weld bead with high accuracy. For the employed DP780 steel, a 1900-2000 ºC temperature range is found to delimit the conduction and keyhole welding mechanisms. Consequently, if a keyhole welding mechanism is desired, it is necessary to guarantee temperatures above 2000ºC during the whole welding process, and vice versa for the conduction welding. Hereafter are summarised the main conclusions.

- In conduction welding the error between the in-situ and ex-situ monitoring is negligible. On the contrary, in keyhole welding, the monitored width presents a small error, as the width value is slightly incremented in comparison with the experimentally measured, ex-situ. However, the monitoring system behaves stable and provides a reliable width value.
- The best process parameters for the studied T-joint welding of the DP780 steel are a 900W laser power and 1100 mm/min feed rate.
- The shear tests confirmed the best welding parameters, given the fact that the joints shear stress is bigger than the base material von Mises shear stress and the punch displacement at failure indicates the welded zone is sufficiently ductile for stamping.

Acknowledgements

The present work was carried out within the IMAGINE Project (Elkartek KK-2021/00120) of the Basque Government. In addition, Predoctoral Programme for the Training of Non-Doctoral Research Staff of the Department of Education of the Basque Government is gratefully acknowledged for its financial support.

References

[1] Gao, S, Li, Y, Yang, L, Qiu, W. Microstructure and mechanical properties of laser-welded dissimilar DP780 and DP980 high-strength steel joints. Materials Science and Engineering: A, 2018,720:117-129.

[2] Wu, D, Zhang, P, Yu, Z, Gao, Y, Zhang, H, Chen, H, Tian, Y. Progress and perspectives of in-situ optical monitoring in laser beam welding: Sensing, characterization and modeling. Journal of Manufacturing Processes, 2022, 75: 767-791.

[3] Krause, T J, Allen, T R, Fraser, J M. Self-witnessing coherent imaging for artifact removal and noise filtering. Optics and Lasers in Engineering, 2022,151:106936.

[4] Allen, T R, Simonds, B J, Tanner, J R, Fraser, J M. Simultaneous in operando monitoring of keyhole depth and absorptance in laser processing of AISI 316 stainless steel at 200 kHz. Procedia CIRP 2020, 94: 419-424.

[5] Xiao, X., Liu, X., Cheng, M., & Song, L. Towards monitoring laser welding process via a coaxial pyrometer. Journal of Materials Processing Technology, 2020, 277: 116409.

[6] Dorsch, F, Braun, H, Keßler, S, Pfitzner, D, Rominger, V. Online characterization of laser beam welds by NIR-camera observation. In High-Power Laser Materials Processing: Lasers, Beam Delivery, Diagnostics, and Applications II, 2013, 8603: 239-250.

[7] Di, H, Sun, Q, Wang, X, Li, J. Microstructure and properties in dissimilar/similar weld joints between DP780 and DP980 steels processed by fiber laser welding. Journal of Materials Science & Technology, 2017, 33(12): 1561-1571.

[8] Köhler, S., Rohnert, C., & Groche, P. (2018). Extension of geometric limits in drawing of stringer sheets. Procedia Manufacturing, 15, 693-700.

[9] Groche, P., & Bäcker, F. (2013). Springback in stringer sheet stretch forming. CIRP Annals, 62(1), 275-278.